AIAA JOURNAL
Vol. 42, No. 1, January 2004

Calculation of Sound Propagation in Nonuniform Flows: Suppression of Instability Waves

Anurag Agarwal* and Philip J. Morris†
Pennsylvania State University, University Park, Pennsylvania 16802
and
Ramani Mani‡
G. E. Global Research Center, Niskayuna, New York 12309

Acoustic waves propagating through nonuniform flows are subject to convection and refraction. Most noise prediction schemes use a linear wave operator to capture these effects. However, the wave operator can also support instability waves that, for a jet, are the well-known Kelvin–Helmholtz instabilities. These are convective instabilities that can completely overwhelm the acoustic solution downstream of the source location. A general technique to filter out the instability waves is presented. A mathematical analysis is presented that demonstrates that the instabilities are suppressed if a time-harmonic response is assumed, and the governing equations are solved by a direct solver in the frequency domain. Also, a buffer-zone treatment for a nonreflecting boundary condition implementation in the frequency domain is developed. The outgoing waves are damped in the buffer zone simply by adding imaginary values of appropriate sign to the required real frequency of the response. An analytical solution to a one-dimensional model problem, as well as numerical and analytical solutions to a two-dimensional jet instability problem, are provided. They demonstrate the effectiveness, robustness, and simplicity of the present technique.

I. Introduction

MANY noise prediction schemes use a two-step process to predict sound from turbulent flows. First, the sources are characterized, perhaps in terms of amplitude, length, and timescales obtained from a Reynolds-averaged Navier–Stokes solution. Then, the sound generated by these sources is calculated as it propagates through the sheared mean flow to eventually reach the observer outside the source region. This paper addresses the second step: how to propagate the sound from the source to the observer. The method developed here is appropriate for relatively low frequencies though its application is general. At high frequencies methods based on ray acoustics or other asymptotic methods are likely to be more efficient.

Sources of sound immersed in a jet generate acoustic waves that are convected and refracted as they propagate through the jet shear layer. The acoustic perturbations are so small compared to the mean (base) state that their contribution to the jet flow itself is negligible. Thus, the acoustic waves can be described by linearizing the fluid flow equations (Navier–Stokes) about the mean flow. Moreover, because viscosity has a negligible effect on sound propagation the viscous terms can also be neglected. This results in the selection of the Euler equations linearized about the mean flow, which in one form or another have become the de facto standard for noise-propagation prediction schemes.

Unfortunately, in addition to acoustic waves, the linearized Euler equations also support instability waves that, for a jet, are the well-known Kelvin–Helmholtz instabilities. These are convective instabilities in which the disturbances grow as they propagate downstream from the point of introduction. The instability-wave solution can completely overwhelm the acoustic-wave solution. Thus, it is imperative for an accurate noise prediction scheme to filter out the instability wave. In the complete physical problem the instabilities contribute to the turbulence and are limited and modified by nonlinear and viscous effects. In that sense within the framework of the linearized Euler equations the instabilities are nonphysical if the actual problem to be solved is for sound propagation in a turbulent sheared flow. It should be remembered that the inhomogeneous linearized Euler equations only represent a mathematical model of a part of the physical problem.

One of the first theoretical studies of mean-flow refraction effects was performed by Gottlieb,[1] who obtained far-field acoustic solutions from a line and a point source placed near a vortex sheet. The solution was obtained by first integrating the plane waves over the wave numbers that make up the source. The resulting field integrals for the solution were evaluated by the method of stationary phase to obtain far-field approximations. The Kelvin–Helmholtz instability appears as a pole in the complex wave-number plane that was neglected by Gottlieb to obtain only the acoustic-wave solution. Mani[2] used the same technique to predict refraction effects on acoustic waves produced by a point source embedded in a jet that was modeled by a plug flow. The same procedure was used by Tester and Burrin[3] to obtain the far-field acoustic radiation from a point source immersed in an infinitely parallel jet. Following a more formal approach, Dowling et al.[4] showed that such acoustic solutions that neglect the instability wave solution are weakly causal in that they violate causality to maintain finiteness.

Unfortunately, realistic three-dimensional jets do not lend themselves to such analytical simplifications by which the instability waves can be ignored. Asymptotic methods such as the geometrical acoustics approach can be used for this purpose because they do not suffer from the instability problem. However, this approximate method is restricted to high-frequency waves, and it fails to predict accurately some important mean flow refraction effects in a jet including the behavior inside the zone of silence. Ewert et al.[5] proposed a set of acoustic perturbation equations to calculate sound propagation through nonuniform flows. They state that the resulting perturbation solution is free of instabilities. This is not

Presented as Paper 2003-0878 at the 41st Aerospace Sciences Meeting, Reno, NV, 6 January 2003; received 30 January 2003; revision received 14 August 2003; accepted for publication 22 August 2003.

*Graduate Research Assistant, Department of Aerospace Engineering. Student Member AIAA.
†Boeing/A. D. Welliver Professor, Department of Aerospace Engineering. Fellow AIAA.
‡Chief Technologist, Aeroacoustics, Energy and Propulsion Technologies, One Research Circle. Associate Fellow AIAA.

surprising because the wave operator for the acoustic perturbation equations matches the approximate wave operator derived previously by Pierce,[6] which is valid only for flowfields that are slowly varying relative to an acoustic wavelength (high-frequency limit). In fact, Pierce[6] shows that the approximate wave operator can be reduced to the geometrical acoustics equations, thus restricting its application to relatively high frequencies. In another effort to suppress the instability wave solution of the linearized Euler equations, Bailly et al.[7] removed some of the mean shear terms from the linearized Euler equations. Such a procedure is nonphysical, and its accuracy in capturing the mean flow refraction effects is uncertain. Hence, all of these approximate methods have a limited range of validity and can fail at low frequencies.

The objective of the present paper is to develop a global approach to suppress the unwanted instability waves from the linearized Euler equations. Through a detailed mathematical analysis, it is shown in Sec. II that if appropriate boundary conditions are implemented the instability waves can be suppressed from the solutions of the linearized Euler equations simply by seeking a solution in the frequency domain.

In Sec. III, an analytical solution for a one-dimensional model problem of the coupling of two waves with different group velocities is given. It is shown that if the problem is solved in the space–time domain for a time-harmonic source, after posing it as an initial value problem, a convectively unstable response is obtained. However, if the response is assumed to be time harmonic at the source frequency and the problem is solved in the frequency domain a stable response is obtained.

Finally, in Sec. IV, a more physically relevant example of sound propagation from a time-harmonic source immersed in a two-dimensional jet is considered. The jet is subject to a Kelvin–Helmholtz instability for the given source frequency. It is shown that the instability is captured accurately by an explicit time-marching solver. However, in the present approach it is desired to filter out this unwanted instability wave and only examine the propagation of acoustic waves. Following the theory developed in Sec. II, it is shown that this is accomplished if the response is assumed to be time harmonic and if the ensuing time-independent partial differential equations are solved in space. Because the computational domain is finite in extent, appropriate boundary conditions need to be implemented. To this end, a buffer domain treatment in the frequency domain has been developed to allow for a nonreflecting passage of the outgoing waves. To implement this boundary condition, the physical domain of interest is surrounded by an artificial region (a buffer zone). In this buffer zone the outgoing waves are forced to decay exponentially by adding imaginary parts of appropriate sign to the assumed real frequency of the response. For reasons explained next, it is shown that these boundary conditions ensure boundedness in space and provide absorbing (nonreflecting) boundaries.

II. General Theory

Consider the following partial differential equation in one space dimension x:

$$L\left(\frac{\partial}{\partial x}, \frac{\partial}{\partial t}, x\right) g(x,t) = \delta(x) e^{-i\omega_0 t} \tag{1}$$

where L is a differential operator that is linear in time t and has no explicit dependence on t, $g(x,t)$ is the Green's function for a time-harmonic source, and $\delta(\,)$ is the Dirac delta function.

Equation (1) can be posed as an initial-value problem, and then its response $g(x,t)$ can be obtained. Alternatively, the response can be assumed to be time harmonic with the source frequency because the L operator is linear and independent of t. That is, $g(x,t) = \hat{g}(x)\exp[-i\omega_0 t]$. Thus, the time-dependent terms can be factored out, and the resulting time-independent equations can be posed as a boundary-value problem. These two cases are treated separately in the following two subsections.

A. Space–Time Response: Solution to the Initial-Value Problem

The analysis in this subsection is based on the theory of absolute and convective instabilities that has been studied by several authors in the past (e.g., Briggs,[8] Bers,[9] and Huerre and Monkewitz[10]). Only some of the key ideas from the theory are described here for completeness.

For simplicity, it is assumed that the medium is homogeneous and of infinite extent. Application of the Fourier–Laplace transform defined by

$$U(k,\omega) = \int_{-\infty}^{\infty} \mathrm{d}x e^{-ikx} \int_{0}^{\infty} \mathrm{d}t e^{i\omega t} u(x,t) \tag{2}$$

to Eq. (1) yields

$$D(k,\omega)G(k,\omega) = i/(\omega - \omega_0) \tag{3}$$

The space–time response is recovered by an application of the inverse Fourier–Laplace transform

$$g(x,t) = \int_F \frac{\mathrm{d}k}{2\pi} e^{ikx} \int_L \frac{\mathrm{d}\omega}{2\pi} e^{-i\omega t} \frac{i}{D(k,\omega)(\omega - \omega_0)} \tag{4}$$

where $D(k,\omega) = 0$ is the dispersion relation that either maps a wave number k into the ω plane $[\omega(k)]$ or vice versa $[k(\omega)]$. F is the inverse Fourier contour that is chosen to be the real k axis (k_r) (Fig. 1a). L is the inverse Laplace contour. For the response to be causal, the L contour is placed above all of the singularities

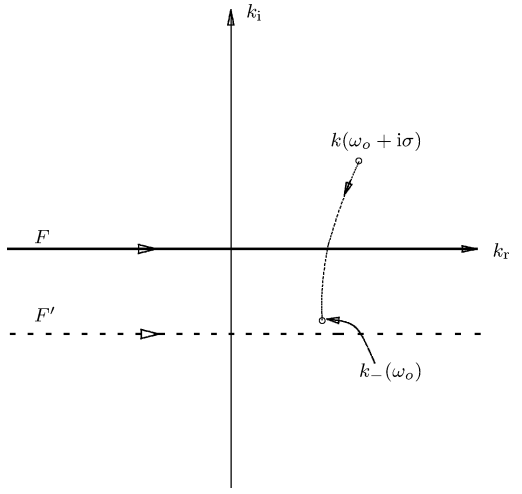

a) k plane

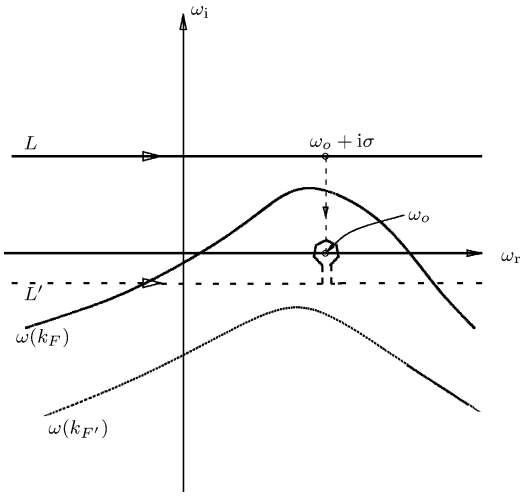

b) ω plane

Fig. 1 Lowering of the inverse Fourier contour from $F \rightarrow F'$ in conjunction with the inverse Laplace contour from $L \rightarrow L'$. The inverse Laplace-contours lie above the respective $\omega(k)$ maps to maintain causality. The residue at ω_0 dominates the time-asymptotic response.

$[\omega(k_F), \omega_0]$ in the ω plane (see Fig. 1b). Note that the zeroes of the dispersion relation represent singularities in the integrand of Eq. (4). Now the integration contour is closed at infinity in the upper-half ω plane for $t < 0$, and from Cauchy's theorem this gives a zero result, thus satisfying causality. The medium is unstable to perturbations if for any k_F, $\Im[\omega(k_F)] > 0$. This can be seen by the application of the Method of Residues for $t > 0$. An analytical evaluation of the integrals in Eq. (4) for an unstable case is presented next.

B. Unstable Response

Because $\Im[\omega(k_F)] > 0$ ($\Im$ denotes the imaginary part) for some k_F, to maintain causality the L contour is placed above the highest point of the map $\omega(k_F)$ in the upper-half ω plane. We are interested in the response after the transients have subsided ($t \to \infty$). Such an asymptotic evaluation becomes amenable to analytical evaluation if the L contour can be deformed to a location L' just below the ω_r axis, except near the pole at ω_0 as shown in Fig. 1b. Then the large time-asymptotic response is dominated by the residue evaluated at the pole at ω_0 because the residues evaluated at all of the other poles below L' yield exponentially decaying solutions in time. However, the L contour will intersect the map $\omega(k_F)$ in the ω plane if it is lowered towards the ω_r axis. This would violate causality. To prevent this, the F contour must be lowered in the k plane in conjunction with the deformation of the L contour. Let F' be the location of the deformed inverse-Fourier contour that allows the L contour to be lowered to the L' contour while maintaining causality. Now that the integration contour has been analytically continued to a position below the ω_r axis to L', it can be closed at infinity in the lower-half ω plane for $t > 0$, and the time-asymptotic response is given by the residue at $\omega = \omega_0$, which from Eq. (4) is

$$g(x, t \to \infty) = \int_{F'} \frac{\mathrm{d}k}{2\pi} \frac{e^{i(kx - \omega_0 t)}}{D(k, \omega_0)} \tag{5}$$

(It has been assumed that there are no branch points in the upper-half ω plane that would give rise to absolute instabilities.[9] Hence the instability is implicitly assumed to be convective. However, the ideas in the present paper are valid for absolutely unstable systems as well.) For simplicity, it is assumed that $D(k, \omega_0)$ has a simple zero, $k_-(\omega_0)$, where the negative subscript indicates that $\Im[k] < 0$. If $\Im[k(\omega_0 + i\sigma)] > 0$, where σ is a real, positive quantity such that $\omega_0 + i\sigma$ lies on L, then it is clear that the $k_-(\omega_0)$ root in the k plane originated in the upper-half k plane and that it has been moved to the lower-half k plane by the contour deformation procedure. Because $k(\omega_0 + i\sigma)$ was above the F contour, $k_-(\omega_0)$ lies above the F' contour. For $x > 0$ the integration contour is closed in the k plane above the F' contour, and after the application of the Method of Residues the integral in Eq. (5) can be evaluated as

$$g(x, t \to \infty) = -i \frac{e^{i[k_-(\omega_0)x - \omega_0 t]}}{\partial D/\partial k[k_-(\omega_0), \omega_0]} H(x) \tag{6}$$

where $H(\,)$ is the Heaviside function. This response is exponentially growing in the $+x$ direction.

If ω_0 does not lie below $\omega(k_F)$, then $k(\omega_0)$ will remain in the upper-half k plane, leading to a stable time-asymptotic response. Thus a convectively unstable system is time asymptotically unstable in space only for a limited range of source frequencies.

In the preceding analysis it has been assumed that there is single instability mode that is growing and traveling in the $+x$ direction, but the analysis can be readily generalized to all possible cases.

C. Assumed Time-Harmonic Response

The assumed time-harmonic response can be represented as

$$g(x, t) = \hat{g}(x) e^{-i\omega_0 t} \tag{7}$$

The time dependence in Eq. (1) can be removed by replacing $\partial/\partial t \to -i\omega_0$ and factoring out the $\exp[-i\omega_0 t]$ term from both sides to give

$$L\left(\frac{\partial}{\partial x}, x; \omega_0\right) \hat{g}(x) = \delta(x) \tag{8}$$

Application of the Fourier transform (denoted by a tilde) to this equation gives

$$D(k; \omega_0) \tilde{\hat{g}}(k; \omega_0) = 1 \tag{9}$$

The dispersion relation $D(k; \omega_0)$ is the same as in Eq. (3) but with $\omega \to \omega_0$. Also, because the time dependence is lost the inverse-Fourier contour becomes independent of the inverse-Laplace contour. Hence, the inverse Fourier-contour does not have to be deformed and is chosen to be along the real k axis. The spatial response is recovered by an application of the inverse-Fourier transform

$$\hat{g}(x; \omega_0) = \int_{-\infty}^{\infty} \frac{\mathrm{d}k}{2\pi} \frac{e^{ikx}}{D(k; \omega_0)} \tag{10}$$

As in the preceding subsection, it is assumed that $k_-(\omega_0)$ is the only root of the dispersion relation. To evaluate the integral in Eq. (10), the integration contour can be closed in the upper- (lower-)half k plane for $x > 0$ ($x < 0$), and after the application of the method of residues, we obtain

$$\hat{g}(x; \omega_0) = -i \frac{e^{ik_-(\omega_0)x}}{\partial D/\partial k[k_-(\omega_0); \omega_0]} H(-x) \tag{11}$$

The final assumed time-harmonic response is obtained from Eq. (7). This is an exponentially decaying response for $x < 0$. Thus the exponentially growing solution for $x > 0$ for the space–time response is converted into an exponentially decaying response for $x < 0$. Therefore, the assumed time-harmonic response is stable. Assuming a time-harmonic response with a real frequency is equivalent to forcing the L contour to remain on the real ω axis. Thus, if the space–time initial-value problem is unstable then causality is violated by the assumed time-harmonic response. Because causality is violated only for unstable solutions, it is still satisfied for the acoustic-wave solution. This must be true because the two solutions are independent.

In the following section a simple model problem is used first to demonstrate how an instability can be suppressed. This is followed by a more relevant physical problem involving an acoustic source embedded in a plane, infinitely parallel jet flow. It is shown how the Kelvin–Helmholtz instability in the jet can be suppressed by the present solution method while the acoustic solution is preserved. The present technique can also be used for nonparallel, three-dimensional mean flows.

III. One-Dimensional Example

Consider the following differential equation:

$$\frac{\partial^2 f}{\partial t^2} + 3\frac{\partial^2 f}{\partial t \partial x} + 2\frac{\partial^2 f}{\partial x^2} - \gamma^2 f = 0 \tag{12}$$

where γ^2 is a positive real constant that couples together two waves of group velocities $+2$ and $+1$, respectively. This simple physical example exhibits convective instability. The impulse response of this system was provided by Bers.[9] In this section the space–time and assumed time-harmonic responses to a periodic forcing of Eq. (12) are provided.

A. Space–Time Response

The space–time Green's function to a time-harmonic source is given by the differential equation

$$\left\{\frac{\partial^2}{\partial t^2} + 3\frac{\partial^2}{\partial t \partial x} + 2\frac{\partial^2}{\partial x^2} - \gamma^2\right\} g(x, t) = \delta(x) e^{-i\omega_0 t} \tag{13}$$

The solution is given by (see Sec. A in Appendix A)

$$g(x, t) = \left[-e^{-i\omega_0 (t - 3x/4)} \big/ \lambda\right] \{e^{\lambda x/4} - e^{-\lambda x/4}\} H(x) \tag{14}$$

where $\lambda = \sqrt{(8\gamma^2 - \omega_0^2)}$. Equation (14) represents a growing response in x but only when $\lambda \in \mathbb{R}$ ($\mathbb{R}$ denotes the real-number space), that is, $\omega_0 < \sqrt{(8)}\gamma$. This is in agreement with the earlier noted characteristic of a convectively unstable system, which is unstable for only a definite range of source frequencies.

B. Assumed Time-Harmonic Response

The governing equation for this case is the same as Eq. (13), but it is assumed that $g(x,t) = \hat{g}(x;\omega_0)e^{-i\omega_0 t}$. The final solution is given by (see Sec. B in Appendix A)

$$g(x,t) = \frac{e^{-i\omega_0(t-3x/4)}}{\lambda} \times \begin{cases} e^{-\lambda x/4} : x > 0 \\ -e^{\lambda x/4} : x < 0 \end{cases} \tag{15}$$

where $\lambda = \sqrt{(8\gamma^2 - \omega_0^2)}$. Hence, as expected, the assumed time-harmonic response is stable for all source frequencies.

IV. Sound Propagation Through a Two-Dimensional Jet

In this example a time-harmonic energy source is immersed in a two-dimensional jet that generates an acoustic wave that is refracted as it moves through the jet shear layer. In addition, an instability wave is excited in the jet shear layer that propagates in the direction downstream of the source.

For a parallel jet the linearized continuity, momentum, energy, and the equation of state for a perfect gas can be simplified and written in the following form:

$$\mathrm{L}\left(\frac{\partial}{\partial \boldsymbol{x}}, \frac{\partial}{\partial t}, \boldsymbol{x}\right)\boldsymbol{U}(\boldsymbol{x},t) = \boldsymbol{S}(\boldsymbol{x})\cos(\omega_0 t) \tag{16}$$

where

$$\mathrm{L} = \begin{bmatrix} \boxdot & \bar{\rho}(y)\dfrac{\partial}{\partial x} & \dfrac{\mathrm{d}\bar{\rho}(y)}{\mathrm{d}y} + \bar{\rho}(y)\dfrac{\partial}{\partial y} & 0 \\ 0 & \boxdot & \dfrac{\mathrm{d}\bar{u}(y)}{\mathrm{d}y} & \dfrac{1}{\bar{\rho}(y)}\dfrac{\partial}{\partial x} \\ 0 & 0 & \boxdot & \dfrac{1}{\bar{\rho}(y)}\dfrac{\partial}{\partial y} \\ 0 & \gamma\bar{p}\dfrac{\partial}{\partial x} & \gamma\bar{p}\dfrac{\partial}{\partial y} & \boxdot \end{bmatrix}$$

$$\boldsymbol{U} = \begin{Bmatrix} \rho \\ u \\ v \\ p \end{Bmatrix}, \qquad \boldsymbol{S} = \begin{Bmatrix} 0 \\ 0 \\ 0 \\ \Lambda(\boldsymbol{x}) \end{Bmatrix} \tag{17}$$

where $\boxdot = \partial/\partial t + \bar{u}(y)\partial/\partial x$, $\Lambda(\boldsymbol{x}) = A\exp[-(B_x x^2 + B_y y^2)]$. The mean flow variables are denoted by an overbar and are given by

$$\bar{u}(y) = u_j e^{-(\ell_n 2)(y/b)^2} \tag{18}$$

$$\frac{1}{\bar{\rho}(y)} = -\frac{1}{2}\frac{\gamma-1}{\gamma\bar{p}}[\bar{u}(y) - u_j]\bar{u}(y) + \frac{1}{\rho_j}\frac{\bar{u}(y)}{u_j} + \frac{1}{\rho_\infty}\frac{u_j - \bar{u}(y)}{u_j} \tag{19}$$

where $\bar{p} = \text{constant} = 103{,}330\ \mathrm{m^{-1}\ kg\ s^{-2}}$. The parameters for the problem are selected to be $M_j = 0.756$, $T_j = 600$ K, $T_\infty = 300$ K, $R = 287.0\ \mathrm{m^2\ s^{-2}\ K^{-1}}$, $\gamma = 1.4$, $b = 1.3$ m, $A = 0.001\ \mathrm{kgm^{-1}\ s^{-3}}$, $B_x = 0.04\ \ell_n(2)\ \mathrm{m^{-2}}$, $B_y = 0.32\ \ell_n(2)\ \mathrm{m^{-2}}$, where $M_j = u_j/a_j$ and $a_j = (\gamma R T_j)^{1/2}$. The source frequency $\omega_0 = 76$ rad/s.

Equation (16) can be solved in the space–time domain by using an explicit time-marching scheme, or by assuming a time-harmonic response in the frequency domain. Depending on the source frequency, these techniques can yield different results as explained next.

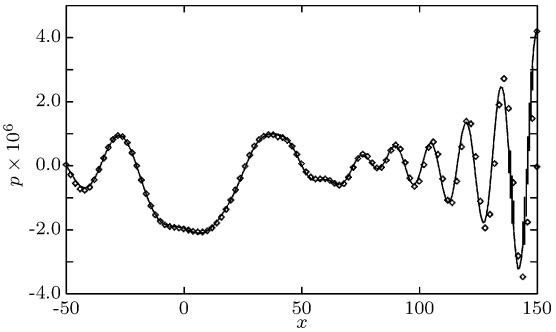

Fig. 2 Comparison of the analytical solution (◇) along the sideline $y = 15$ with numerical solution (——) obtained by a space–time solver.

A. Space–Time Solution

First, the linearized Euler equations are solved in the space–time domain by an explicit finite-difference scheme. A fourth-order dispersion-relation-preserving scheme is used for spatial discretization, and a fourth-order Runge–Kutta scheme is used for time integration (see Agarwal and Morris[11] for the numerical implementation details and boundary treatment). The given source frequency excites an instability wave. This is accurately captured by the space–time solver as can be seen in Fig. 2, which compares the numerical solution on the line $y = 15$ with the analytical solution (given in Appendix B). The solution exhibits a growing spatial instability. The numerical and analytical solutions agree well.

B. Assumed Time-Harmonic Response

Here, the response is assumed to be time harmonic. That is,

$$\boldsymbol{U}(\boldsymbol{x},t) = \boldsymbol{U}(\boldsymbol{x};\omega)e^{-i\omega_0 t} \tag{20}$$

if the source term in Eq. (16) is made complex. Then the governing equation for the response is given by

$$\mathrm{L}\left(\frac{\partial}{\partial \boldsymbol{x}}, \frac{\partial}{\partial t}, \boldsymbol{x}\right)\boldsymbol{U}(\boldsymbol{x},t) = \boldsymbol{S}(\boldsymbol{x})\exp[-i\omega_0 t] \tag{21}$$

with the understanding that the physical response is given by the real part of the solution. After the substitution of Eq. (20) into Eq. (21), replacing the time-derivative terms $\partial/\partial t \to -i\omega_0$ and factoring out the $\exp[-i\omega_0 t]$ term from both sides of the resulting equation, the resulting system of equations can be manipulated to eliminate all of the dependent variables in favor of the perturbation pressure p. This results in the following partial differential equation:

$$\left\{D^3 - \bar{c}^2(y)\left[D\nabla^2 - \frac{1}{\bar{\rho}(y)}\frac{\mathrm{d}\bar{\rho}(y)}{\mathrm{d}y}D\frac{\partial}{\partial y} - 2\frac{\mathrm{d}\bar{u}(y)}{\mathrm{d}y}\frac{\partial^2}{\partial x \partial y}\right]\right\}p = D^2\Lambda(\boldsymbol{x}) \tag{22}$$

where $D = (-i\omega_0 + \bar{u}\partial/\partial x)$ and $\nabla^2 = \partial^2/\partial x^2 + \partial^2/\partial y^2$. The operator on p in Eq. (22) is also known as Lilley's wave operator.[12] This equation is solved here in space by a direct frequency-domain solver. Note that the present technique is also applicable to the linearized Euler equations in their component form. The component equations have been reduced to a single equation only for simplicity.

The computational domain is the interval $[x_{\min}, x_{\max}] \times [y_{\min}, y_{\max}] = [-250, 225] \times [0, 100]$. A symmetry boundary condition is applied along the line $y = 0$. The left and top boundaries must absorb the outgoing acoustic wave. The right boundary must absorb the acoustic, vorticity, and entropy waves that are generated by the source. Also, the left boundary must accommodate an incoming wave (see Appendix B for details). To allow for a clean passage of the outgoing waves (no reflection), a buffer domain treatment has been developed in the frequency domain. The basic step in the application of this boundary condition involves surrounding the physical domain of interest by a buffer domain in which the waves are forced to decay exponentially away from the source, so that at the outer

edge of the buffer domain the waves have decayed to a negligible value.

The exponential decay in the buffer domain is achieved by replacing the assumed frequency of the response ω_0 by a complex frequency of the form

$$\beta(\boldsymbol{x}) = \omega_0 + i\,\sigma(\boldsymbol{x}) \tag{23}$$

where $\sigma(\boldsymbol{x})$ is zero within the physical domain and takes on real positive values for outgoing waves in the buffer domain. Numerical experiments performed on different benchmark problems reveal that the length of the buffer domain must be at least two wavelengths of the outgoing wave.

The damping function σ must be chosen so that its slope is zero at the edge of the physical domain and its value rises gradually to a maximum at the domain's outer edge. For the present calculations the damping function is chosen to be an exponential function. For a one-dimensional problem the damping function takes the form

$$\sigma(x) = \mu\omega_0 \frac{1 - \exp\left[\kappa x_b(x)^2\right]}{1 - \exp[\kappa]} \tag{24}$$

where x_b is a buffer domain coordinate that is 0 at the beginning of the buffer domain and 1 at the end and has a linear variation in between and μ and κ are constants with values of 2 and 4, respectively. For a two-dimensional domain the damping function is shaped like an inverted tablecloth.

The rationale behind the use of the frequency distribution of Eq. (23) can be understood by assuming that the imaginary part of the frequency varies slowly over a wavelength of the outgoing wave. This is easily accomplished by controlling the parameter κ and the length of the buffer domain. Based on this assumption, local Fourier analysis can be carried out for the local (constant) frequency. For outgoing waves it is observed from the dispersion relation that increasing the imaginary part of the initially real frequency changes the real wave number into a complex number such that the outgoing waves are damped. Because the frequency is real in the physical domain, the solution is unaffected in this region, but is gradually damped in the buffer domain. For example, consider an outgoing plane acoustic wave traveling in the $+x$ direction. Such a wave can be written as $p(x,t) = p(x;\omega_0)\exp[-i\omega_0 t]$, where the assumed time-harmonic response is given by

$$p(x;\omega_0) = \exp[ikx] \tag{25}$$

The wave number k is given by the dispersion relation $k = \omega_0/c$. Now if ω_0 is replaced by $\beta(x) = \omega_0 + i\sigma(x)$, where $\sigma(x)$ is given by Eq. (24), then k is transformed into a complex number with a positive imaginary part. From Eq. (25) this clearly represents a decaying response in the $+x$ direction. The same argument holds for a wave traveling in the $-x$ direction. Thus, the damping zones provide nonreflecting (absorbing) boundaries for the outgoing waves by increasingly damping them as they propagate through the buffer domain. Near the outer edge of the buffer zones, the waves decay to a negligible value. Hence a Dirichlet boundary condition $p = 0$ can be applied along the outer edge of the computational domain. The damping zones are effective for outgoing waves. However, they amplify any incoming waves. To accommodate an incoming wave, the left boundary is placed at a sufficient distance from the origin, and the grid is stretched away from the source. Grid stretching damps out high wavenumber waves and thus offsets the amplification produced by the buffer zones. This procedure ensures outgoing acoustic waves from the left-hand boundary while accommodating an incoming wave. Note that the amplitude of the incoming wave is governed by the source strength at the origin and is exponentially decaying in the $-x$ direction. Thus the incoming wave has a negligible contribution to the overall solution. However, the numerical solution is sensitive to the boundary conditions, and it is essential to account for the incoming wave in the boundary treatment.

The computational domain is discretized by a grid that is clustered around $y = 0$ to capture the sharp gradients within the shear layer. The grid is also clustered around $x = 0$, so that it can be stretched out to a reasonable distance upstream and downstream of the source location while providing a better resolution near the source. The required grid layout is obtained by mapping the physical domain into a computational domain by the coordinate transformations (from Ref. 13):

$$\xi = A + \frac{1}{\chi}\sinh^{-1}\left[\left(\frac{x}{D} - 1\right)\sinh(\chi A)\right] \tag{26}$$

$$\eta = 1 - \frac{\log[(\mu + 2 - y/y_{\max})/(\mu - 1 + y/y_{\max})]}{\log[(\mu + 1)/(\mu - 1)]} \tag{27}$$

where

$$A = \frac{1}{2\chi}\log\left[\frac{1 + (\exp[\chi] - 1)(D/L)}{1 + (\exp[-\chi] - 1)(D/L)}\right] \tag{28}$$

The computational domain (ξ, η) consists of uniformly spaced grid points. Then the preimage of ξ and η describes the grid layout in the physical domain. The parameters used for the present simulation are $\chi = 5.0$, $\mu = 1.01$, $D = -x_{\min}$, and $L = x_{\max} - x_{\min}$. A total of $N_x \times N_y = 440 \times 300$ grid points are used. The buffer domain is 70 units deep along the left, top, and right boundaries.

Equation (22) is solved using a finite difference method. The spatial derivatives are approximated by second-order, central-difference formulas. After application of the Dirichlet boundary conditions, the finite difference equations can be written in the following matrix form:

$$\mathrm{S}\cdot\boldsymbol{p} = \boldsymbol{l} \tag{29}$$

There are a total of $N_x \times N_y$ grid points resulting in $N_x \times N_y$ unknowns $p_{i,j}$ that are approximations of the actual function $p(x, y)$ at the grid points (i, j). These unknowns can be put in a one-dimensional sequence to obtain a vector form $\boldsymbol{p} = [p_0, p_1, \ldots, p_{N_x N_y - 1}]^T$, where $p_k = p_{i,j}$ for $k = i + jN_x$. S is a sparse matrix that is banded with left and right bandwidths of $N_x + 1$, and $\boldsymbol{l}$ is the right-hand side (known) or load vector. Further details of the matrix setup can be found in Press et al.[14]

The matrix S is inverted by using a direct matrix inversion method (for example LU decomposition). The resulting solution for pressure is found to be free of instabilities, as expected. Figure 3 shows a comparison between the numerical and the analytical solution for the acoustic waves along the line $y = 15$. Calculations with a coarser grid $N_x \times N_y = 325 \times 300$ showed a small discrepancy with the analytical solution in the vicinity of $x = 0$. This error has been eliminated with the present, higher-resolution grid.

For reasons of efficiency, an alternative solution technique that might be considered in the frequency domain is a time-stepping approach by adding a pseudotime term. To illustrate this technique, consider the linearized Euler equations in the following vector form:

$$\frac{\partial \boldsymbol{U}}{\partial t} + \mathrm{A}(y)\frac{\partial \boldsymbol{U}}{\partial x} + \mathrm{B}(y)\frac{\partial \boldsymbol{U}}{\partial y} = \boldsymbol{S}(x, y)e^{-i\omega_0 t} \tag{30}$$

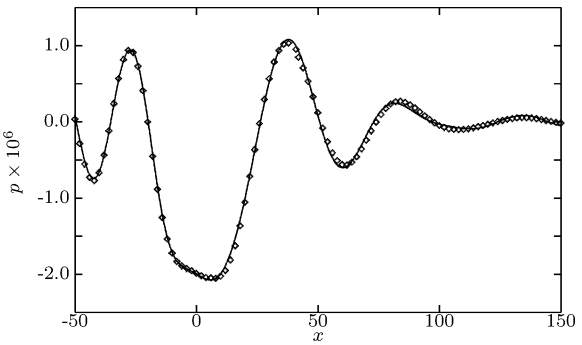

Fig. 3 Comparison of the analytical solution (◇) along the sideline $y = 15$ with numerical solution (——) obtained by a direct, frequency-domain solver.

Let $\boldsymbol{U} = \hat{\boldsymbol{U}}(x;\omega_0)\exp[-i\omega_0 t]$. Then,

$$-i\omega_0\hat{\boldsymbol{U}} + \mathrm{A}(y)\frac{\partial \boldsymbol{U}}{\partial x} + \mathrm{B}(y)\frac{\partial \boldsymbol{U}}{\partial y} = \boldsymbol{S}(x,y) \tag{31}$$

Instead of solving this elliptic equation by a direct solver, after posing it as a boundary-value problem, it can be set up as an initial-value problem by the addition of a pseudotime term:

$$\frac{\partial \hat{\boldsymbol{U}}}{\partial \tau} - i\omega_0\hat{\boldsymbol{U}} + \mathrm{A}(y)\frac{\partial \boldsymbol{U}}{\partial x} + \mathrm{B}(y)\frac{\partial \boldsymbol{U}}{\partial y} = \boldsymbol{S}(x,y) \tag{32}$$

Now this parabolic equation can be solved in the space–time domain by an explicit, time-marching scheme. The response $\hat{\boldsymbol{U}}(x;\omega_0)$ is recovered after the transients have died out, that is, when $\partial\hat{\boldsymbol{U}}/\partial\tau \to 0$.

However, this approach does not filter out the instability waves and, in fact, leads to the same time-asymptotic solution as that obtained in Sec. IV.A. To appreciate this result, let us apply the Fourier–Laplace transform to Eq. (30) to obtain

$$-i\omega\boldsymbol{U} + \mathrm{f}(k,y)\boldsymbol{U} = i\tilde{\boldsymbol{S}}(k,y)/(\omega-\omega_0) \tag{33}$$

where $\mathrm{f}(k,y)$ is the Fourier transform of $\mathrm{A}(y)\partial/\partial x + \mathrm{B}(y)\partial/\partial y$. The dispersion relation is given by equating the determinant of the homogeneous part of this equation to zero, that is,

$$\omega = -i\det[\mathrm{f}(k,y)] \tag{34}$$

If the medium is unstable to perturbations, then for some real k, $\Im[\omega(k_r)] > 0$. Now, consider Eq. (32). Following the same steps as just given, the dispersion relation for this equation is given by

$$\omega = \omega_0 - i\det[\mathrm{f}(k,y)] \tag{35}$$

Note that ω_0 is real. Therefore, if Eq. (30) is unstable to perturbations the same must be true for Eq. (32). Thus, the addition of a pseudo-time term to a frequency-domain formulation and the subsequent space–time solution of the pseudo-initial-value problem maintains causality in pseudotime and does not suppress the instability waves. Iterative algorithms such as Jacobi and Gauss–Siedel methods are equivalent to time-marching methods and would also include the instability wave. Hence, a direct solver must be used to filter out the instabilities.

V. Conclusions

In this paper a general technique to filter out instability-wave solutions from any linear wave operator has been presented. With the present approach sound propagation through nonuniform flows can be calculated without having the instability waves overwhelm the acoustic-wave solution. Earlier procedures to tackle this problem were only approximate, and their range of validity was limited. The present approach is also very simple to implement numerically. It is only necessary to solve the governing equations by a direct solver in the frequency domain. To implement the boundary conditions, the physical domain is surrounded by an artificial buffer zone, in which the outgoing waves are absorbed by adding positive imaginary values to the real frequency ω_0 of the $\exp[-i\omega_0 t]$ response. This method also has an advantage in terms of computational time. A three-dimensional time-domain calculation takes a very long time to converge to a periodic steady-state solution for a given frequency. With the frequency-domain approach the solution is obtained by a single matrix inversion that is computationally more efficient. This, however, is also the disadvantage of this technique because direct matrix solvers for a three-dimensional problem require large amounts of memory, particularly at high frequencies. Fortunately, the memory problem can be resolved by using parallel direct solvers. At high frequencies asymptotic methods like geometrical acoustics can be used.

Appendix A: Coupling of Two Waves—Analytical Solution

A. Space–Time Green's Function

The space–time Green's function for the problem of the coupling of two waves forced by a time-harmonic source is obtained by first finding the impulse response of the system, the governing equation for which is given by

$$\left(\frac{\partial^2}{\partial t^2} + 3\frac{\partial^2}{\partial t\,\partial x} + 2\frac{\partial^2}{\partial x^2} - \gamma^2\right)g(x,t) = \delta(x-\zeta)\delta(t-\tau) \tag{A1}$$

Because this is a linear equation with constant coefficients, the differential equation can be solved with the source location at the origin, and the Green's function for the general source location is obtained simply by replacing $x \to (x-\zeta)$ and $t \to (t-\tau)$. For convenience, whenever the source is at the origin its location in the argument of the Green's function will be omitted. That is, $g(x,t) \Leftrightarrow g(x,t|0,0)$. This reduces Eq. (A1) to

$$\left(\frac{\partial^2}{\partial t^2} + 3\frac{\partial^2}{\partial t\,\partial x} + 2\frac{\partial^2}{\partial x^2} - \gamma^2\right)g(x,t) = \delta(x)\delta(t) \tag{A2}$$

Application of the Fourier–Laplace transform defined in Eq. (2) to the preceding equation yields

$$[D(k,\omega)]G(k,\omega) = 1 \tag{A3}$$

where $D(k,\omega)$ is given by

$$D(k,\omega) = -(\omega-2k)(\omega-k) - \gamma^2 \tag{A4}$$

The space–time Green's function is recovered by the application of the inverse Fourier–Laplace transform to Eq. (A3):

$$g(x,t) = \int_L \frac{\mathrm{d}\omega}{2\pi}e^{-i\omega t}\int_F \frac{\mathrm{d}k}{2\pi}e^{ikx}\frac{1}{D(k,\omega)} \tag{A5}$$

where F is the inverse Fourier contour that is taken to be the k_r axis. To maintain causality, the inverse Laplace contour L is placed above the largest positive imaginary value of the roots of the dispersion relation $D(k_r,\omega) = 0$ that are given by

$$\omega(k_r) = \left(3k_r \pm \sqrt{k_r^2 - 4\gamma^2}\right)\Big/2 \tag{A6}$$

It is clear that in the range $|k_r| < 2\gamma$ there is a branch of ω for which $\omega_i > 0$. This implies that the system is unstable.

Using Eq. (A6), Eq. (A5) for the Green's function can be written as

$$g(x,t) = -\int_{-\infty}^{\infty}\frac{\mathrm{d}k}{2\pi}e^{ikx}I(k,t) \tag{A7}$$

where

$$I(k,t) = \int_L \frac{\mathrm{d}\omega}{2\pi}e^{-i\omega t}\frac{1}{\omega - \left(3k \pm \sqrt{k^2-4\gamma^2}\right)\Big/2} \tag{A8}$$

This integral is evaluated using the method of residues to give

$$I(k,t) = \left(2\Big/\sqrt{k^2-4\gamma^2}\right)\sin\left[\left(\sqrt{k^2-4\gamma^2}\Big/2\right)t\right]e^{-i\frac{3}{2}kt}H(t) \tag{A9}$$

Using Eq. (A9), the integral in Eq. (A7) can be evaluated exactly as (see Gradshteyn and Ryzhik[15])

$$g(x,t) = I_0\left[\sqrt{8}\gamma\sqrt{t-x/2}\sqrt{x-t}\,\right]\times H[(x-t)(2t-x)] \tag{A10}$$

where I_0 is the modified Bessel function of the first kind. This solution represents a traveling pulse. For an observer moving with a speed $V = x/t$, such that $1 < V < 2$, Eq. (A10) can be simplified to

$$g\left(x, t = \frac{x}{V}\right) = I_0[\Gamma x] = 1 + \sum_{n=1}^{\infty} \frac{\left[\frac{1}{4}(\Gamma x)^2\right]^n}{(n!)^2} \tag{A11}$$

where $\Gamma = \sqrt{(8)}\gamma[(1 - V/2)(V - 1)/V]^{1/2}$ is a real positive quantity. Clearly this represents a convectively unstable response.

The Green's function for a time-harmonic source is given by the differential equation

$$\left(\frac{\partial^2}{\partial t^2} + 3\frac{\partial^2}{\partial t\,\partial x} + 2\frac{\partial^2}{\partial x^2} - \gamma^2\right)\bar{g}(x, t; \omega_0) = \delta(x)e^{-i\omega_0 t} \tag{A12}$$

This Green's function is easily obtained by the following convolution in terms of the impulse-response Green's function:

$$\bar{g}(x, t) = \int_0^{\infty} g(x, t|0, t_0)e^{-i\omega_0 t_0}\,\mathrm{d}t_0, \qquad (t - t_0) < x < 2(t - t_0) \tag{A13}$$

Substituting Eq. (A10) into Eq. (A13) yields

$$\bar{g}(x, t) = \int_0^{\infty} I_0\left[\sqrt{8}\gamma\sqrt{(t - t_0) - \frac{x}{2}}\sqrt{x - (t - t_0)}\right]e^{-i\omega_0 t_0}\,\mathrm{d}t_0 \times H(t - t_0) \tag{A14}$$

Let $z = 3x/4 - (t - t_0)$. This simplifies the preceding integral to

$$\bar{g}(x, t) = e^{-i\omega_0[t - 3(x/4)]} \times \int_{-x/4}^{x/4} J_0\left(-\sqrt{8}\gamma\sqrt{z^2 - \frac{x^2}{16}}\right)e^{-i\omega_0 z}\,\mathrm{d}z \tag{A15}$$

The integral in Eq. (A15) can be evaluated (see Gradshteyn and Ryzhik[15]), giving

$$\bar{g}(x, t) = 2e^{-i\omega_0[t - 3(x/4)]}\frac{\sin\left[(x/4)\sqrt{\omega_0^2 - 8\gamma^2}\right]}{\sqrt{\omega_0^2 - 8\gamma^2}} \tag{A16}$$

Letting $\lambda = \sqrt{(8\gamma^2 - \omega_0^2)}$ ($\lambda \in \mathbb{R}$ for instability), we obtain

$$\bar{g}(x, t) = \left(-e^{-i\omega_0(t - 3x/4)}\big/\lambda\right)(e^{\lambda x/4} - e^{-\lambda x/4})H(x) \tag{A17}$$

B. Assumed Time-Harmonic, Constant-Frequency Response

Because the differential equation (A12) is linear and the coefficients are time-independent, $\bar{g}(x, t)$ can be assumed to be periodic in time with the frequency given by that of the source. That is,

$$\bar{g}(x, t) = \hat{g}(x; \omega_0)e^{-i\omega_0 t} \tag{A18}$$

This simplifies Eq. (A12) to

$$\left(-\omega_0^2 - 3i\omega_0\frac{\partial}{\partial x} + 2\frac{\partial^2}{\partial x^2} - \gamma^2\right)\hat{g}(x; \omega_0) = \delta(x) \tag{A19}$$

Application of the Fourier transform to Eq. (A19) gives

$$[D(k, \omega_0)]\hat{g}(k; \omega_0) = 1 \tag{A20}$$

where $D(k, \omega)$ is given by Eq. (A4). The assumed time-harmonic Green's function is obtained by the application of the inverse Fourier transform to Eq. (A20):

$$\hat{g}(x; \omega_0) = \int_{-\infty}^{\infty} \frac{\mathrm{d}k}{2\pi}e^{ikx}\frac{1}{D(k, \omega_0)} \tag{A21}$$

The upper- and lower-half k-plane roots of $D(k, \omega_0)$ are given by

$$k_{\pm} = (3\omega_0 \pm \lambda i)/4 \tag{A22}$$

For $x > 0$ ($x < 0$) the integration contour is closed in the upper- (lower-) half k plane, and after the application of the method of residues the following expression for the assumed time-harmonic response is obtained:

$$\bar{g}(x, t) = \hat{g}(x; \omega_0)e^{-i\omega_0 t} = \frac{e^{-i\omega_0(t - 3x/4)}}{\lambda}\begin{cases} e^{-\lambda x/4} : x > 0 \\ -e^{\lambda x/4} : x < 0 \end{cases} \tag{A23}$$

Appendix B: Analytical Solution to Lilley's Equation

For a time-harmonic source Lilley's equation in the frequency domain can be written as

$$\left\{D^3 - \bar{c}^2(y)\left[D\nabla^2 - \frac{1}{\bar{\rho}(y)}\frac{\mathrm{d}\bar{\rho}(y)}{\mathrm{d}y}D\frac{\partial}{\partial y} - 2\frac{\mathrm{d}\bar{u}(y)}{\mathrm{d}y}\frac{\partial^2}{\partial x\,\partial y}\right]\right\}p = D^2 S \tag{B1}$$

where $D = (-i\omega + \bar{u}\partial/\partial x)$, $\nabla^2 = \partial^2/\partial x^2 + \partial^2/\partial y^2$, $S = A\exp[-B(x^2 + y^2)]$, ω is the source frequency, x is the streamwise coordinate, y is the cross-stream coordinate. The mean flow variables are functions of y only and are represented by an overbar. The mean pressure $\bar{p}$ is constant, and the mean speed of sound is given by $\bar{c}(y) = \{\gamma\bar{p}/\bar{\rho}(y)\}^{1/2}$.

Application of the Fourier transform defined by

$$\tilde{p}(k, y) = \int_{-\infty}^{\infty} p(x, y)e^{-ikx}\,\mathrm{d}x \tag{B2}$$

to Eq. (B1) and some rearrangement yields

$$\frac{\mathrm{d}^2\tilde{p}}{\mathrm{d}y^2} + \left[\frac{2k}{\omega - k\bar{u}(y)}\frac{\mathrm{d}\bar{u}(y)}{\mathrm{d}y} - \frac{1}{\bar{\rho}(y)}\frac{\mathrm{d}\bar{\rho}}{\mathrm{d}y}\right]\frac{\mathrm{d}\tilde{p}}{\mathrm{d}y} + \left\{\frac{[\omega - k\bar{u}(y)]^2}{\bar{c}(y)^2} - k^2\right\}\tilde{p} = \frac{i\tilde{S}}{\bar{c}^2(y)}[\omega - k\bar{u}(y)] \tag{B3}$$

The operator on the left-hand side of Eq. (B3) is the compressible Rayleigh operator, also known as the Pridmore–Brown operator $\tilde{S} = A(\pi/B)^{1/2}\exp[-k^2/(4B) - By^2]$ is the Fourier transform of the source S. Equation (B3) can be rearranged in the following self-adjoint form:

$$-\frac{\mathrm{d}}{\mathrm{d}y}\left[b(k, y)\frac{\mathrm{d}}{\mathrm{d}y}\right]\tilde{p} + q(k, y)\tilde{p} = \bar{S}(k, y) \tag{B4}$$

where $b(k, y) = -1/[\tilde{D}^2\bar{\rho}(y)]$, $\bar{S}(k, y) = -\tilde{S}/[\tilde{D}\bar{\rho}(y)\bar{c}^2(y)]$, $q(k, y) = -k^2/(\tilde{D}^2\bar{\rho}) - 1/(\bar{\rho}\bar{c}^2)$, and $\tilde{D} = (-i\omega + ik\bar{u})$. The Green's function for Eq. (B4) satisfies the following equation:

$$-\frac{\mathrm{d}}{\mathrm{d}y}\left[b(k, y)\frac{\mathrm{d}}{\mathrm{d}y}\right]G(k, y|y_0) + q(k, y)G(k, y|y_0) = \delta(y - y_0) \tag{B5}$$

together with the boundary conditions

$$\frac{\mathrm{d}G(k, 0)}{\mathrm{d}y} = 0, \qquad G(k, y \to \infty) = \exp[-\nu y] \tag{B6}$$

where $\nu = [k^2 - k_{\infty}^2]^{1/2}$ and $k_{\infty} = \omega/c_{\infty}$ and c_{∞} is the sound speed in the ambient medium. The locations of the branch cuts in the k plane associated with ν are shown in Fig. B1, and the branch of the square root is chosen such that $\nu(0) = -ik_{\infty}$. Let ϕ_1 and ϕ_2 be two linearly independent solutions for the homogeneous form of Eq. (B5) such that ϕ_1 satisfies the first boundary condition and ϕ_2 satisfies the other. The Green's function is a combination of these

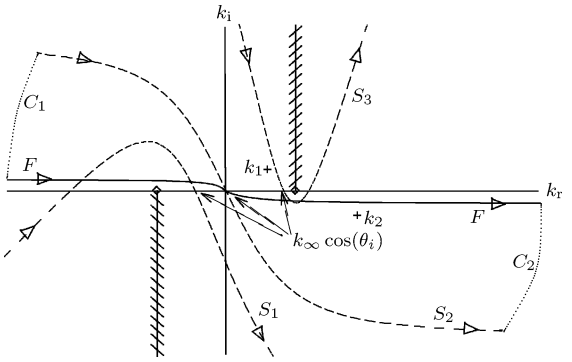

Fig. B1 Location of the inverse-Fourier contour F and the steepest-descent paths S_i in the k plane. Also shown are the locations of the branch points (◇) and branch cuts (++++) of ν and the eigenvalues of Eq. (B3) (marked +).

functions that is continuous at $y = y_0$ and has a jump in its derivative of $-1/b(k, y)$ at y_0. Thus, we obtain

$$G(k, y|y_0) = [1/J(\phi_1, \phi_2)][\phi_1(y)\phi_2(y_0)H(y_0 - y) + \phi_2(y)\phi_1(y_0)H(y - y_0)] \tag{B7}$$

where $H(\,)$ is the Heaviside function and $J(\phi_1, \phi_2)$ is the conjunct of the two solutions given by

$$J(\phi_1, \phi_2) = b(k, y_0)[\phi_1'(y_0)\phi_2(y_0) - \phi_1(y_0)\phi_2'(y_0)] \tag{B8}$$

Note that J is independent of y_0 (compare Theorem 7.1 of Ref. 16).

The solution to Eq. (B1) is obtained by the application of the inverse Fourier transform to the convolution of the Green's function with the source. Thus,

$$p(x, y) = \int_F \frac{\mathrm{d}k}{2\pi} e^{ikx} \int_0^\infty G(k, y|y_0)\bar{S}(k, y_0)\,\mathrm{d}y_0 = \frac{-iA}{2\pi\gamma\bar{P}}\sqrt{\frac{\pi}{B}}[I_1 + I_2] \tag{B9}$$

$$I_1 = \int_F \phi_2(k, y)e^{-k^2/4B} \times \frac{1}{J}\left\{\int_0^y \frac{\phi_1(k, y_0)e^{-By_0^2}}{[\omega - k\bar{u}(y_0)]}\,\mathrm{d}y_0\right\} e^{ikx}\,\mathrm{d}k$$

$$I_2 = \int_F \phi_1(k, y)e^{-k^2/4B} \times \frac{1}{J}\left\{\int_y^\infty \frac{\phi_2(k, y_0)e^{-By_0^2}}{[\omega - k\bar{u}(y_0)]}\,\mathrm{d}y_0\right\} e^{ikx}\,\mathrm{d}k \tag{B10}$$

where F is the Fourier contour and its location in the k plane is shown in Fig. B1. Note that for this choice of F only the acoustic-wave solution is obtained. For a causal response that captures the instability wave as well, the F contour must pass below the Kelvin–Helmholtz instability pole k_2.

The integrals in Eq. (B9) will be evaluated along the sideline $y = 15$. On this line $I_2 \approx 0$ because $\exp[-By_0^2] \approx 0$ in the interval $15 \le y_0 \le \infty$. Therefore, only I_1 needs to be evaluated. Also, at $y = 15$ $\bar{u} \approx 0$; hence, $\phi_2 = \exp[-\nu y]$. (ϕ_1 needs to be evaluated numerically.) Therefore,

$$p(x, y) = \frac{-iA}{2\pi\gamma\bar{P}}\sqrt{\frac{\pi}{B}}\int_F e^{-k^2/4B}\frac{1}{J} \times \left\{\int_0^y \frac{\phi_1(k, y_0)e^{-By_0^2}}{[\omega - k\bar{u}(y_0)]}\,\mathrm{d}y_0\right\} e^{ikx - \nu y}\,\mathrm{d}k \tag{B11}$$

Numerical evaluation of the preceding integrals in its present form is extremely difficult. This is because on the F contour $\exp[ikx]$ becomes increasingly oscillatory with increasing modulus of k. This poses a convergence issue for any integration scheme. To overcome this oscillatory behavior, the F contour is deformed onto the path of steepest descent. The following is an extension of the procedure given by Noble.[17]

Let $x = r\cos\theta$, $y = r\sin\theta$, and $0 < \theta < \pi$. Then using the coordinate transformation

$$k = k_\infty \cos\beta, \qquad \beta \in \mathbb{C} \tag{B12}$$

yields

$$ikx - \nu y = ik_\infty r\cos[\beta - \theta] \tag{B13}$$

On the steepest descent path

$$ik_\infty \cos[\beta - \theta] = -u^2 + ik_\infty, \qquad u \in \mathbb{R} \tag{B14}$$

This implies that

$$k(u) = k_\infty \cos\left\{\theta \pm \arccos\left[i\left(u^2/k_\infty\right) + 1\right]\right\} \tag{B15}$$

where the positive (negative) sign is used for negative (positive) values of u. Therefore, Eq. (B11) is transformed into

$$p(x, y) = \frac{A}{\pi\gamma\bar{P}}\sqrt{\frac{\pi}{B}}e^{irk_\infty}k_\infty \int_{S_i} e^{-k(u)^2/4B}\frac{1}{J[k(u)]} \times \left\{\int_0^y \frac{\phi_1[k(u), y_0]e^{-By_0^2}}{[\omega - k\bar{u}(y_0)]}\,\mathrm{d}y_0\right\} \times \frac{\sin[\lambda(u)]}{\sqrt{u^2 - 2ik_\infty}} e^{-ru^2}\,\mathrm{d}u \tag{B16}$$

with $\lambda(u) = \theta + \arccos(iu^2/k_\infty + 1)$. From Eq. (B15) it is clear that the steepest descent paths are a function of θ (observer locations). Figure B1 shows the steepest descent paths S_i for three different observer locations: S_1 for $\theta_1 > \pi/2$, S_2 for $\theta_2 = \pi/2$, and S_3 for $\theta_3 < \pi/2$. Every S_i path crosses the real k axis at $k_\infty\cos(\theta_i)$ and at $k_\infty/\cos(\theta_i)$. Because the branch points of ν ($\pm k_\infty$) always lie between these two points, the associated branch cuts of ν are chosen in the direction shown in Fig. B1. This ensures that the S_i paths do not cross the branch cuts. To understand how the F contour can be transformed into an S_i path, consider the steepest descent path S_2. Because the original F contour is being deformed into S_2, the two contours can be connected by arcs at infinity (C_1 and C_2). It can be shown that the integrals on the arcs at infinity are zero, so that

$$\int_F = \int_{S_2} \pm 2\pi i \sum_{i=1}^{n} \mathrm{Res}(k_i) \tag{B17}$$

where the last term represents a summation over all of the residues evaluated at the poles that are crossed over while deforming the F contour into the steepest-descent contour. The poles in the integrand of Eq. (B11) [or Eq. (B16)] satisfy the condition

$$J(k) = 0 \tag{B18}$$

From Eq. (B8) this means that $\phi_1 = \phi_2$. In other words, ϕ_1 (or ϕ_2) is a solution of the compressible Rayleigh equation [homogeneous form of Eq. (B3)] that satisfies both the boundary conditions [Eq. (B6)]. Therefore, such solutions must be the eigenfunctions, and the wave numbers k that satisfy Eq. (B18) must be the eigenvalues of the compressible Rayleigh equation. For this problem there are two eigenvalues for the compressible Rayleigh equation, one lies in the upper-half k plane k_1 and other in the lower-half plane k_2 (Fig. B1). The residue at either of the poles k_i is given by

$$\mathrm{Res}(k_i) = \frac{-iA}{2\pi\gamma\bar{P}}\sqrt{\frac{\pi}{B}}e^{-k_i^2/4B}\frac{1}{\mathrm{d}J(k_i)/\mathrm{d}k} \times \left\{\int_0^y \frac{\phi_1(k_i, y_0)e^{-By_0^2}}{[\omega - k_i\bar{u}(y_0)]}\,\mathrm{d}y_0\right\} e^{ik_i x - \nu y} \tag{B19}$$

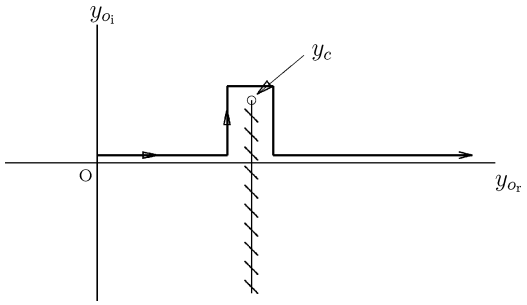

Fig. B2 Location of the critical point y_c and the branch cut for the logarithmic singularity in Eq. (B3).

Note that the term within the braces is independent of x and needs to be evaluated only once along the line $y = 15$. For a causal response $\mathrm{Res}(k_2)$ contributes to the solution for $x > 0$, thus yielding an exponentially growing solution. However, for a noncausal assumed time-harmonic response $\mathrm{Res}(k_2)$ contributes to the solution for $x < 0$. This is an incoming wave (traveling towards the source) that decays exponentially away from the source.

Caution must be exercised while evaluating the y_0 integrals in Eqs. (B16) and (B19) because Eq. (B3) has a regular singular point at y_c given by $\omega - k\bar{u}(y_c) = 0$. For the velocity profile in the present problem,

$$y_c = b\left\{\frac{\log(kU_j/\omega)}{\log(2.0)}\right\}^{\frac{1}{2}} \tag{B20}$$

Application of the method of Frobenius reveals that Eq. (B3) has a logarithmic singularity at y_c. Following the mathematical analysis by Lin,[18] it can be shown that for the present case the logarithmic branch cut must connect y_c and infinity in the lower half y_0 plane. The integration path in the y_0 plane might have to be deformed from the real y_0 axis to avoid this branch cut (Fig. B2). Another issue is the branch cut in the k plane associated with the square-root function in Eq. (B20). To resolve this, note that for $\theta < \pi/2$, on the steepest-descent path, y_c is always real and positive at the point $k_\infty/\cos(\theta)$. Once the branch of the square root in Eq. (B20) has been determined at this point, the same branch can be used for all other points on the steepest-descent contour. Thus, given the steepest-descent path the branch cut for the square-root function must be selected in such a manner that it is not crossed by the steepest-descent path. For $\theta > \pi/2$, y_c lies in the lower-half y_0 plane, and hence the integration can be carried out on the real y_0 axis.

Now the perturbation pressure on the sideline of the jet given by Eq. (B11) is well defined and can be evaluated with the help of Eqs. (B16), (B17), and (B19).

Acknowledgments

This work is supported in part by the NASA Langley Research Center under Grant NAG1-01-009 (with Technical Monitor Mehdi Khorrami). A. Agarwal also acknowledges the support of the summer internship awarded to him by the G. E. Global Research Center.

References

[1]Gottlieb, P., "Sound Source near a Velocity Discontinuity," *Journal of the Acoustical Society of America*, Vol. 32, No. 9, 1960, pp. 1117–1122.

[2]Mani, R., "The Influence of Jet Flow on Jet Noise. Part 1. The Noise of Unheated Jets," *Journal of Fluid Mechanics*, Vol. 73, No. 4, 1976, pp. 753–778.

[3]Tester, B. J., and Burrin, R. H., "On Sound Radiation from Sources in Parallel Sheared Jet Flows," AIAA Paper 74-57, Jan. 1974.

[4]Dowling, A. P., Ffowcs Williams, J. E., and Goldstein, M. E., "Sound Production in a Moving Stream," *Philosophical Transactions of the Royal Society of London, A*, Vol. 288, 1978, pp. 321–349.

[5]Ewert, R., Meinke, M., and Schröder, W., "Computation of Trailing Edge Noise via LES and Acoustic Perturbation Equations," AIAA Paper 2002-2467, June 2002.

[6]Pierce, A. D., "Wave Equation for Sound in Fluids with Unsteady Inhomogeneous Flow," *Journal of the Acoustical Society of America*, Vol. 87, No. 6, 1990, pp. 2292–2299.

[7]Bailly, C., Bogey, C., and Juvé, D., "Computation of Flow Noise Using Source Terms in Linearized Euler's Equations," *AIAA Journal*, Vol. 40, No. 2, 2002, pp. 235–243.

[8]Briggs, R. J., *Electron-Stream Interaction with Plasmas*, MIT Press, Cambridge, MA, 1964, Chap. 3.

[9]Bers, A., *Handbook of Plasma Physics*, Vol. 1, North-Holland, Amsterdam, 1983, Chap. 3.2.

[10]Huerre, P., and Monkewitz, P., "Local and Global Instabilities in Spatially Developing Flows," *Annual Review of Fluid Mechanics*, Vol. 22, 1990, pp. 473–537.

[11]Agarwal, A., and Morris, P. J., "Generation and Radiation of Acoustic Waves from a 2-D Shear Layer," *Third Computational Aeroacoustics (CAA) Workshop on Benchmark Problems*, NASA CP 2000-209790, 2000, pp. 309–314.

[12]Lilley, G. M., "The Generation and Radiation of Supersonic Jet Noise. Vol IV—Theory of Turbulence Generated Jet Noise, Noise Radiation from Upstream Sources and Combustion Noise," U.S. Air Force Aero Propulsion Lab., TR-72-53, Wright–Patterson AFB, OH, July 1972 (available from Defence Technical Information Center as AD 749 139).

[13]Hoffmann, K. A., and Chiang, S. T., *Computational Fluid Dynamics for Engineers*, Engineering Education System, Wichita, KS, 1989, Chap. 9.

[14]Press, W., Flannery, B., Teukolsky, S., and Vetterling, W., *Numerical Recipes in C++: the Art of Scientific Computing*, Cambridge Univ. Press, Cambridge, England, U.K., 2002, Chap. 19.

[15]Gradshteyn, I. S., and Ryzhik, I. M., *Table of Integrals, Series and Products*, Academic Press, New York, 2000, Chaps. 3 and 4.

[16]Roach, G. F., *Green's Functions*, Cambridge Univ. Press, Cambridge, England, U.K., 1999, Chap. 7.

[17]Noble, B., *Methods Based on the Wiener-Hopf Techniqe*, Chelsea Publishing Co., 1988, Chap. 1.

[18]Lin, C. C., *The Theory of Hydrodynamic Stability*, Cambridge Univ. Press, 1955, Chap. 8.

A. Karagozian
Associate Editor